*Anal. Chem.* **2008,** *80,* 5695–5705

*Accelerated Articles*

# Direct Electrical Transduction of Antibody Binding to a Covalent Virus Layer Using Electrochemical Impedance

**Li-Mei C. Yang, Juan E. Diaz, Theresa M. McIntire, Gregory A. Weiss,* and Reginald M. Penner***

*Department of Chemistry, University of California, Irvine, California 92697-2025*

**Electrochemical impedance spectroscopy is used to detect the binding of a 148.2 kDa antibody to a "covalent virus layer" (CVL) immobilized on a gold electrode. The CVL consisted of M13 phage particles covalently anchored to a 3 mm diameter gold disk electrode. The ability of the CVL to distinguish this antibody ("p-Ab") from a second, nonbinding antibody ("n-Ab") was evaluated as a function of the frequency and phase of the measured current relative to the applied voltage. The binding of p-Ab to the CVL was correlated with a change in the resistance, reducing it at low frequency (1−40 Hz) while increasing it at high frequency (2−140 kHz). The capacitance of the CVL was virtually uncorrelated with p-Ab binding. At both low and high frequency, the electrode resistance was linearly dependent on the p-Ab concentration from 20 to 266 nM but noise compromised the reproducibility of the p-Ab measurement at frequencies below 40 Hz. A "signal-to-noise" ratio for antibody detection was computed based upon the ratio between the measured resistance change upon p-Ab binding and the standard deviation of this change obtained from multiple measurements. In spite of the fact that the impedance change upon p-Ab binding in the low frequency domain was more than 100 times larger than that measured at high frequency, the S/N ratio at high frequency was higher and virtually independent of frequency from 4 to 140 kHz. Attempts to release p-Ab from the CVL using 0.05 M HCl, as previously described for mass-based detection, caused a loss of sensitivity that may be associated with a transition of these phage particles within the CVL from a linear to a coiled conformation at low pH.**

Whole virus particles prepared using the techniques of phage display[1,2] can function as receptors in biosensors. This has been demonstrated by recent work from our laboratories[3,4] and from others.[5–10] In this application, the receptors are actually polypeptide moieties or epitopes that are appended to the native coat proteins comprising the viral capsid. Thus, multiple receptors are arrayed on the exterior surface of each virus, which are usually filamentous bacteriophages with dimensions of approximately 1 $\mu$m (length) × 6 nm (diameter). Phage-displayed peptide epitopes produced from state-of-the-art libraries[11] have $>10^{10}$ unique peptide sequences and can bind a particular target molecule with an affinity ($K_D > 10^{-10}$ M), on-rate ($k_a > 10^5$ $M^{-1}$ $s^{-1}$), and selectivity that rivals monoclonal antibodies. However, these viruses can be produced in quantity more cheaply and more rapidly. In spite of these attributes, it must be recognized that the evaluation of virus particles as bioaffinity media is still at a very early stage.

* To whom correspondence should be addressed. E-mail: gweiss@uci.edu (G.A.W.); rmpenner@uci.edu (R.M.P.).

(1) Smith, G. *Science* **1985**, *228*, 1315–1317.
(2) Smith, G.; Petrenko, V. *Chem. Rev.* **1997**, *97*, 391–410.
(3) Yang, L. C.; Tam, P. Y.; Murray, B. J.; McIntire, T. M.; Overstreet, C. M.; Weiss, G. A.; Penner, R. M. *Anal. Chem.* **2006**, *78*, 3265–3270.
(4) Yang, L.-M. C.; Diaz, J. E.; McIntire, T. M.; Weiss, G. A.; Penner, R. M. *Anal. Chem.* **2008**, *80*, 933–943.
(5) Nanduri, V.; Bhunia, A. K.; Tu, S.-I.; Paoli, G. C.; Brewster, J. D. *Biosens. Bioelectron.* **2007**, *23*, 248–252.
(6) Nanduri, V.; Sorokulova, I. B.; Samoylov, A. M.; Simonian, A. L.; Petrenko, V. A.; Vodyanoy, V. *Biosens. Bioelectron.* **2007**, *22*, 986–992.
(7) Olsen, E. V.; Sorokulova, I. B.; Petrenko, V. A.; Chen, I. H.; Barbaree, J. M.; Vodyanoy, V. J. *Biosens. Bioelectron.* **2006**, *21*, 1434–1442.
(8) Vodyanoy, V. J.; Pathirana, S. T.; Hartell, M. G.; Olsen, E. V.; Barbaree, J.; Neely, W. C.; Chin, B. A. *Biophys. J.* **2000**, *78*, 267A–267A
(9) Goldman, E.; Pazirandeh, M.; Mauro, J.; King, K.; Frey, J.; Anderson, G. *J. Mol. Recognit.* **2000**, *13*, 382–387.
(10) Petrenko, V. A. *Microelectron. J.* **2008**, *39*, 202–207.
(11) Sidu, S. S.; Weiss, G. A. *Phage Display: A Practical Approach*; Oxford University Press: New York, 2004; pp 27−41.

10.1021/ac8008109 CCC: $40.75 
Published on Web 07/01/2008

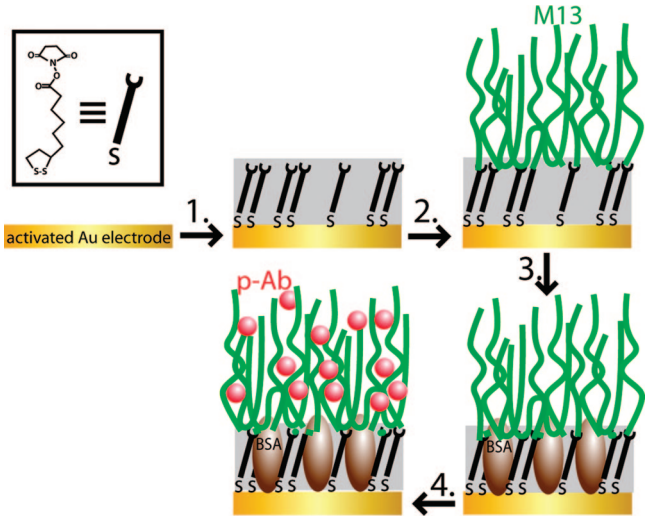


**Figure 1.** Schematic diagram depicting the stepwise assembly of the covalent virus layer, CVL.

To exploit viruses as receptors in biosensors, they must be anchored to a surface. It is essential that these anchored virus particles exhibit a high degree of stability against desorption while retaining the ability of "free" virus particles to recognize and bind a particular target molecule. Recently,[3,4,12] we have developed a protocol (Figure 1) for covalently attaching M13 virus particles to gold surfaces. An assessment of the resulting "covalent virus layer" or CVL using a quartz crystal microbalance in conjunction with a flow cell revealed[4] the following attributes: (1) The CVL is robust. For example, p-Ab in flowing, high ionic strength (150 mM) buffer remained detectible for up to 14 h; (2) The number of binding sites present in the CVL is $\approx 10^{13}$ cm$^{-2}$; (3) The on-rate for p-Ab binding, $k_a \approx 10^4$ M$^{-1}$ s$^{-1}$; and (4) The equilibrium dissociation constant, $K_D \approx 10^{-9}$ M. In addition, we demonstrated that bound antibody could be released from the CVL by exposure to aliquots of 0.5 M HCl. In the QCM evaluation, repeated treatments with 0.5 M HCl produced no diminution of the binding affinity of the CVL for the anti-P8 antibody. Although the performance of the CVL in this study is extremely encouraging, we emphasize that the model system investigated in that study and also in this one represents a best case scenario for phage-displayed receptors: The target molecule is a 148 kDa antibody for the P8 coat protein. Approximately 2700 copies of this protein are present at the surface of each M13 virus particle. In contrast, the "copy number" of displayed peptide epitopes per virus particle would typically be in the range from 5 to 500.

Can electrochemical impedance spectroscopy (EIS) be used instead of QCM to transduce binding to the CVL, as shown in Figure 2? Previously, EIS has often been used in conjunction with redox probes, such as $Fe(CN)_6^{3-/4-}$, and the electron transfer resistance has been monitored to indirectly detect the binding of an analyte molecule.[13–18] Here we focus attention on the label-free detection of biomolecules using an affinity layer in the absence of any added redox probes. Because neither the target molecules nor the affinity layers are electroactive, we rely exclusively on the non-Faradaic impedance of the surface for our EIS "signal". We will attempt to identify conditions of frequency

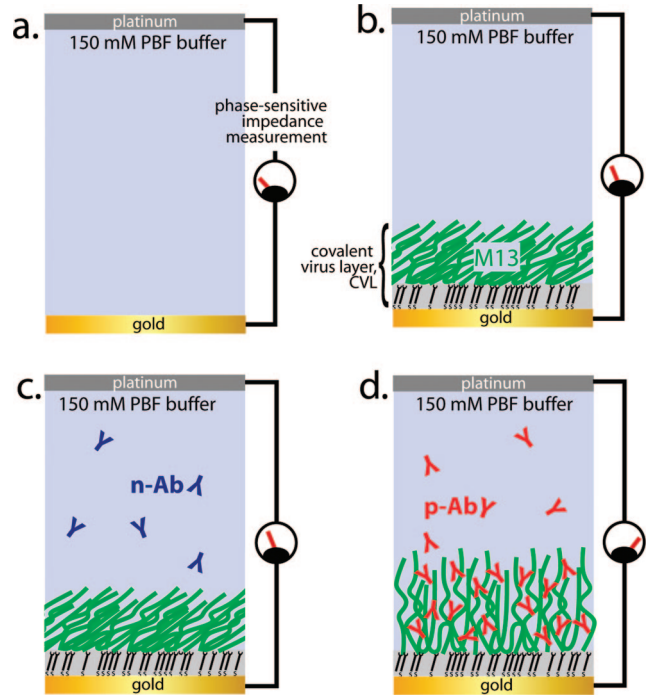


**Figure 2.** Schematic representation of the system investigated here. We seek to identify conditions of frequency and phase for the impedance measurement that enables the most sensitive and reproducible detection of antibody binding to the covalent virus layer, CVL. (a) Bare gold in PBF solution. (b) Virus M13 covalently bound on bare gold electrode via NHS-TE linkers. (c) Anti-FLAG M2 antibody, n-Ab, scarcely bound to CVL. (d) p-Ab bound within CVL.

and phase that permit the detection of antibody binding to the CVL with the highest sensitivity and selectivity. In prior biosensing experiments of this type in which EIS has been used to transduce binding to an immobilized receptor, the low frequency ($f < 1$ Hz) capacitance has most often been exploited for detection.[19–21] This approach suffers from poor temporal resolution and it is susceptible to low frequency noise that can predominate in these measurements. Hamers and co-workers[22] measured the impedance of modified-diamond electrodes at an intermediate frequency of 200 Hz and reported shifts in both the resistance and the capacitance with the binding of an antibody at this frequency. Similarly, DeSilva et al. monitored the binding of staphylococcus enterotoxin B (SAB) to immobilized antibodies of SAB at 100 Hz in the absence of added redox species.[23] In an earlier, preliminary investigation of the CVL,[3] we concluded that the EIS could be employed to detect both the P8 antibody and a second target

(12) Diaz, J. E.; Yang, L. C.; Lamboy, J. A.; Penner, R. M.; Weiss, G. A. *Methods Biotechnol.*, in press

(13) Liu, J.; Tian, S.; Nielsen, P.; Knoll, W. *Chem. Commun.* **2005**, 2969–2971.
(14) Zhang, S.; Huang, F.; Liu, B.; Ding, J.; Xu, X.; Kong, J. *Talanta* **2007**, *71*, 874–881.
(15) Yan, F.; Sadik, O. *Anal. Chem.* **2001**, *73*, 5272–5280.
(16) Yan, F.; Sadik, O. *J. Am. Chem. Soc.* **2001**, *123*, 11335–11340.
(17) Yang, L.; Li, Y.; Erf, G. *Anal. Chem.* **2004**, *76*, 1107–1113.
(18) Ruan, C.; Yang, L.; Li, Y. *Anal. Chem.* **2002**, *74*, 4814–4820.
(19) Pejcic, B.; De Marco, R. *Electrochim. Acta* **2006**, *51*, 6217–6229.
(20) Lasseter, T.; Cai, W.; Hamers, R. *Analyst* **2004**, *129*, 3–8.
(21) Maalouf, R.; Fournier-Wirth, C.; Coste, J.; Chebib, H.; Saikali, Y.; Vittori, O.; Errachid, A.; Cloarec, J.-P.; Martelet, C.; Jaffrezic-Renault, N. *Anal. Chem.* **2007**, *79*, 4879–4886.
(22) Yang, W.; Butler, J. E.; Russell, J. N., Jr.; Hamers, R. J. *Analyst* **2007**, *132*, 296–306.
(23) Desilve, M. S.; Zhang, Y.; Hesketh, P. J.; Maclay, G. J.; Gendel, S. M.; Stetter, J. R. *Biosens. Bioelectron.* **1995**, *10*, 675–682.

molecule, prostate-specific membrane antigen (PSMA), a promising marker for prostate cancer at high frequencies, above 2 kHz.

Now we look systematically at the electrochemical response of the CVL to p-Ab by measuring the impedance of the virus electrode as a function of the p-Ab concentration in the frequency range from 0.1 Hz to 1 MHz. This analysis leads to two interesting and somewhat unexpected conclusions: First, the resistance of the CVL layer measured at high frequencies, between 4 and 140 kHz, increases slightly (by <10 Ω) and in direct proportion to the concentration of p-Ab in a contacting buffer solution. Second, in spite of the fact that much larger impedance changes (larger by a factor of $10^6$ Ω!) are seen at low frequencies, < 1 Hz, the measurement-to-measurement precision of the resistance increase caused by p-Ab binding is much better in the range from 4 to 140 kHz than at any other frequency range, leading to a superior signal-to-noise ratio for the detection of p-Ab by EIS. The reproducibility of the measurement and the CVL preparation is so good that calibration curves can be constructed for different concentrations of p-Ab by making single measurements using a series of different electrodes.

## EXPERIMENTAL SECTION

**Materials.** All chemicals and solvents (>99% purity) were purchased from Fisher or Merck and used as received, unless noted. DMF and ethanol were dried with 4 Å molecular sieves obtained from Alfa Aesar. The anti-M13 antibody (p-Ab, Amersham Biosciences) and anti-FLAG M2 (n-Ab, Sigma) were used as received. Water for all solutions was processed by a Millipore Milli-Q UV system (resistance >18 MΩ cm). Phosphate buffered fluoride buffer, PBF, (4.2 mM $Na_2HPO_4$, 1.5 mM $KH_2PO_4$, 140 mM NaF, pH 7.2) was filter-sterilized through a 0.22 $\mu$m pore size membrane (Corning). The wash buffer was 0.06% BSA, 0.07% Tween 20 (Sigma) in PBF buffer. BSA (0.2%) in phosphate buffered sodium fluoride (pH 7.2) solution was used for blocking (all percentages provided as w/v). HCl acid wash solutions (0.05 M) were prepared from 2 M HCl diluted with Millipore water and mixed with 0.1% Tween 20.

**Preparation of the Covalent Virus Layer.** This procedure improves upon previously reported procedures.[12] Briefly, circular gold electrodes (3 mm diameter, Bioanalytical Systems, Inc.) were used for this study. Because the placement of the reference electrode relative to the working electrode is critically important, a platinum wire counter electrode was wound tightly around the outside of the plastic, 6 mm diameter cylindrical working electrode body near the working electrode and fixed in position using epoxy as shown in Figure 3. This effectively locked the position of these two electrodes relative to one another and facilitated the transfer of both electrodes between different analyte solutions. The gold working electrode was prepared by polishing it sequentially with 1 $\mu$m and 0.25 $\mu$m diamond compound (Ted Pella) on a microcloth (Buehler), then sonicating it three times in nanopure water for a total of 9 min. Assembly of the CVL on this gold electrode involved four steps (Figure 1):

(1) A self-assembled monolayer of *N*-hydroxy-succinimide thioctic ester (NHS-TE) was prepared on the gold electrode. This was accomplished by incubating the gold electrode for at least 18 h in a solution of 16.5 mM NHS-TE in DMF.

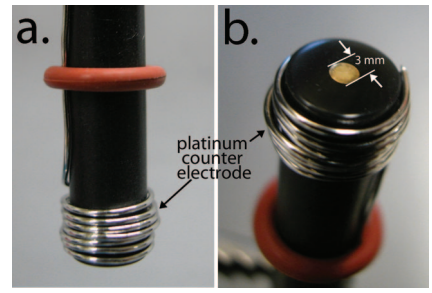


**Figure 3.** Photographs ((a) side view and (b) top view) of the gold working electrode and integral counter electrode used in this study.

(2) M13 virus particles were attached to this NHS-TE modified electrode by incubation in a phage solution (300 $\mu$L, 16 nM in PBF) with shaking for 1 h using an orbital shaker. These electrodes were then rinsed 3 min with PBF followed by an additional 3 min rinse with wash buffer.

(3) These virus immobilized electrodes were blocked with 300 $\mu$L of 0.2% BSA solution with shaking for 40 min and finally rinsed 3 min with wash buffer.

(4) Virus and BSA-modified electrodes were immersed in 300 $\mu$L of aqueous 0.05 M HCl with shaking for 1 min and then rinsed with wash buffer. The purpose of this treatment, which is based upon the results of our earlier work,[4] was to remove weakly bound virus particles and BSA from the surface. Finally, these electrodes were immersed in wash buffer again for an additional 1 min with shaking. The resultant virus electrodes were used immediately to examine analytes of interest.

**Antibody Exposure and Electrochemical Impedance Analysis.** Anti-M13 antibody (p-Ab) and anti-FLAG M2 (n-Ab) antibody were investigated as positive and negative responses against virus M13, respectively. Various concentrations of antibody were prepared with wash buffer prior to exposure to virus electrodes. Preparation of antibody solutions and exposure of the virus electrodes to these solutions involved two steps: First 500 $\mu$L of antibody (either p-Ab or n-Ab) at the desired concentration was prepared in wash buffer. Then the virus electrode was dipped into this "loading" solution for 1 h with shaking. After this hour, the virus electrode was rinsed with wash buffer for 3 min and then transferred to the electrochemical cell containing PBF wash buffer for the impedance measurement.

Each virus electrode was used for one measurement only, corresponding to a single exposure to either p-Ab or n-Ab at the specified concentration and then discarded. Solutions of analytes (n-Ab and p-Ab) were prepared immediately prior to use. All impedance measurements were carried out using a Princeton Applied Research Parstat 2263 potentiostat controlled with the Powersuite module: Powersine software, single sine measurement. The amplitude of the applied voltage modulation was 10 mV, 50 data points in each impedance spectrum were logarithmically sampled and acquired over a frequency range from 1 MHz to 0.1 Hz at the rest potential. For each experiment, involving a single exposure to antibody, triplicate impedance measurements were carried out in rapid succession.

**AFM Analysis.** Intermittent contact mode atomic force microscopy (AFM) imaging was performed in air at ambient pressure

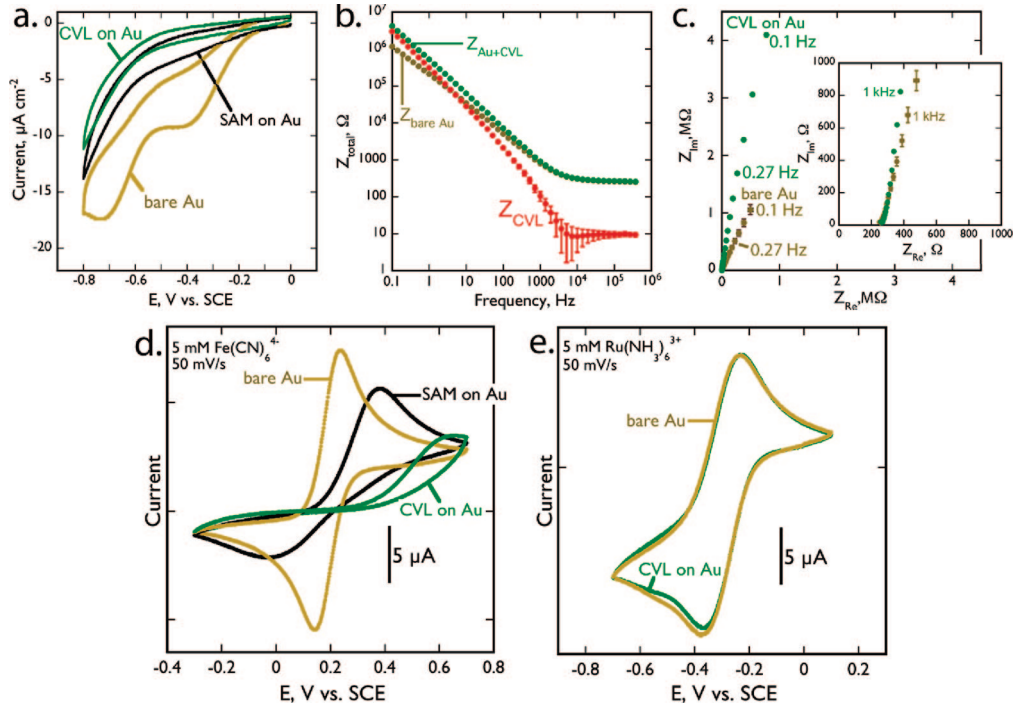


**Figure 4.** (a) Cyclic voltammetry at 20 mV $s^{-1}$ in PBF buffer of a clean bare gold electrode (gold), a SAM-modified gold electrode (black), and a CVL-modified gold electrode (green). (b) Total impedance versus frequency for a bare gold electrode (gold) and an electrode modified by a CVL (green). The difference between these two plots, the total impedance of the CVL, is plotted in red. (c) A Nyquist plot ($Z_{Im}$ versus $Z_{Re}$) for a bare gold electrode and a virus electrode in PBF buffer. The inset shows the data for frequencies above 1 kHz in greater detail. (d) Cyclic voltammetry (50 mV/s) of 5 mM $Fe(CN)_6^{4-}$ at 50 mV/s at a bare gold electrode (gold), a SAM-covered gold electrode (black), and a CVL-covered gold electrode (green). (e) Cyclic voltammetry (50 mV/s) of 5 mM $Ru(NH_3)_6^{3+}$ in PBF buffer at a bare gold electrode (gold) and CVL-covered gold electrodes (green). The CV at a SAM-covered gold electrode was indistinguishable from that at a bare gold electrode.

and humidity using an AutoProbe CP-Research (ThermoMicroscopes, Sunnyvale, CA; now Veeco Instruments, Santa Barbara, CA) scanning probe microscope. The piezoelectric scanner was calibrated using a 5.0 $\mu$m grating in the $x$,$y$, and $z$ directions using an AFM reference (Pacific Nanotechnology, Santa Clara, CA; model no. P-000-0004-0). The AFM tips were silicon (either Multi75 Metrology Probes, model no. MPP-21100; or Tap300 Metrology Probes, model no. MPP-11200, both Veeco Instruments, Santa Barbara, CA). Topographs were obtained as 256 × 256 pixels, flattened line by line, and analyzed using the AutoProbe image processing software supplied by the manufacturer of the AFM. The root-mean-square (rms) surface roughness over selected scanned areas was calculated from the formula $R_{RMS} = [\Sigma(z_n - \bar{z})^2/(N-1)]^{1/2}$, where $\bar{z}$ is the average $z$ height, $z_n$ is the height at each point on the sample, and $N$ is the number of points sampled.

**Dynamic Light Scattering.** Dynamic light scattering (DLS) experiments were performed on a Zetasizer Nano ZS (Malvern Instruments, Southborough, MA), consisting of a 4.0 mW He−Ne laser with a wavelength of 633 nm and a back-scattering angle at 173°. Phosphate buffered saline (PBS, 137 mM NaCl, 3 mM KCl, 8 mM $Na_2HPO_4$, 1.5 mM $KH_2PO_4$, pH 7.2) buffer containing 0.05% Tween-20 was filter-sterilized through a 0.22 $\mu$m pore size membrane (Corning). PBS-Tween solutions were adjusted to pH 2.0 and 4.5 using filter-sterilized 0.1 M HCl. M13 phage were purified twice by PEG-NaCl precipitation and diluted to 50 nM in 1 mL of PBS-Tween solution at pH 2.0, 4.5, and 7.2. Phage samples were allowed to equilibrate in PBS-Tween solutions for 1 h prior to measurement. DLS measurements were collected in 1 mL disposable polystyrene cuvettes at 25 °C, with measurement times of approximately 2 min each and an equilibration time of 3 min between samples. Size distribution results were determined using the built-in DTS software provided by the manufacturer.

## RESULTS AND DISCUSSION

"Virus electrodes" were prepared by assembling a covalent virus layer on a freshly polished gold electrode. The CVL was prepared by first self-assembling a monolayer of *N*-hydroxysuccinimide thioctic (NHS) ester on a clean gold surface (Figure 1). By itself, this self-assembled monolayer (SAM) suppressed most of the current observed in the cyclic voltammogram of a bare gold electrode in the negative potential range from 0 to −0.8 V vs SCE where two reductions attributable to oxygen reduction (≈−0.2 V) and hydrogen evolution (≈−0.6 V) are observed (Figure 4a). Assembly of the CVL was completed by exposing the SAM layer to a solution of M13 in aqueous PBF buffer. Terminal NHS moieties in this monolayer reacted with amines on the surface of the M13 particles to form amide bonds. Previously[4] we estimated the phage "coverage" obtained using this attachment protocol as six equivalent monolayers assuming a phage "footprint" of 1 $\mu$m × 6 nm. The final step in the preparation process is exposure of the bound phage particles to a PBF solution of bovine serium albumin (BSA), a blocking agent that adsorbs on any remaining unprotected gold (Figure 1). A further attenuation of the reduction current seen at the bare gold electrode is observed upon the attachment of phage to the SAM-modifed gold (Figure 4a). The total impedance of the CVL (Figure 4b, red trace) is obtained as the difference between the impedance of the bare gold electrode (Figure 4b, yellow trace) and the virus electrode (green trace). This difference is more than 1 MΩ for frequencies below 1 Hz,

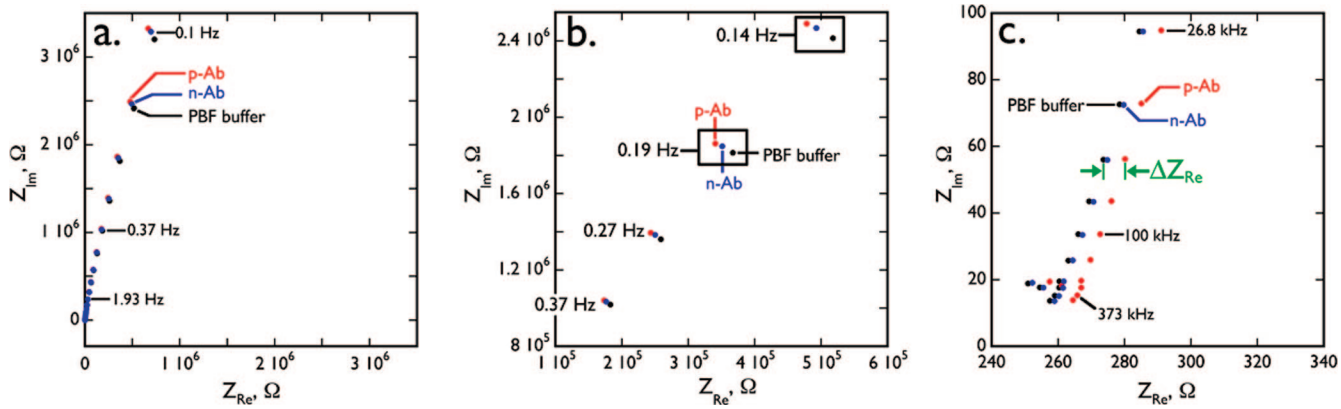


**Figure 5.** Nyquist plots acquired after a 1 h exposure of a CVL first to n-Ab (blue) and then to p-Ab (red). The concentration of both antibodies was 67 nM. Prior to the acquisition of each impedance spectrum, the electrode was transferred into PBF wash buffer for 10 min. (a) Low frequency region, (b) a magnified view of the impedance obtained for four low frequencies, as indicated. (c) A magnified view of the impedance data for frequencies above 26 kHz. An increase in $\Delta Z_{Re}$ is associated with the exposure of the CVL to p-Ab.

but it decreases with increasing frequency to below 4 kHz to just 10 Ω at 4 kHz, and at still higher frequencies, this value is maintained.

A high-frequency impedance of 10 Ω suggests that the CVL, and the SAM layer upon which it is built, are defective and permeable to electrolyte. If this is the case, then the voltammetry of solution phase redox species should be observable. We measured cyclic voltammograms for two: $Ru(NH)_6^{3+}$ and $Fe(CN)_6^{4-}$ (Figure 4d,e). We chose to look at both cationic and anionic redox probes because the CVL itself is negatively charged. The outer surface of the M13 phage is covered with 2700 copies of the protein P8. P8 has three negatively charged residues (Glu2, Asp4, and Asp5) that are exposed at the N-terminus of the protein that is exposed to the solvent.[24,25] Two other fully or partially buried ionic residues (Lys8 and Glu20) near the C-terminus cancel out each other's charge. Thus, each of the 2700 P8 carries a negative charge at pH 7.2 from three carboxylate bearing residues.

In view of this fact, it is not surprising that the voltammetry of these two ions at the virus electrode is different: the oxidation of $Fe(CN)_6^{4-}$ is strongly suppressed at the CVL (Figure 4d), presumably because of the negative charge on the phage particles. At a gold surface covered only with the *N*-hydroxy-succinimide thioctic ester SAM (no phage), the oxidation is 75% as large as at a bare gold electrode (Figure 4d), consistent with the presence of defects in the SAM layer. The voltammetry of $Ru(NH)_6^{2+/3+}$ at the CVL, on the other hand, is hardly attenuated and no difference between a SAM-covered gold electrode and a bare electrode was discernible (data not shown). A description of the CVL consistent with all of the electrochemical data shown in Figure 4 is the following: The defective SAM layer within the CVL blankets 90+% of the gold surface suppressing oxide formation and hydrogen evolution, and both of these processes are expected to produce voltammetric currents that are directly proportional to the exposed gold area. The radial diffusion of solution-phase redox species to pinholes in this SAM monolayer is highly efficient, however, and species like $Ru(NH)_6^{2+/3+}$ amplify the presence of point defects within the SAM. If the radial diffusion fields of adjacent pinholes in the SAM overlap, this ensemble of defects will produce a voltammetric response that is indistinguishable from a bare gold electrode. This is what occurs in the case of $Ru(NH)_6^{2+/3+}$. The amplification of defects by $Fe(CN)_6^{3-/4-}$ is not observed because its concentration at the surface of the SAM and within the negatively charged phage layer is very low as a consequence of Donnan exclusion. The presence of these point defects in the SAM layer also accounts for the very low, 10 Ω series impedance of the CVL at high frequencies.

The partitioning of the total impedance, $Z_{total}$, between the imaginary component of the impedance, $Z_{Im} = 1/\omega C$, and the real component of the impedance, $Z_{Re} = R$, can be seen in a Nyquist plot (Figure 4c). These data show that the increase in $Z_{total}$ seen at low frequencies (Figure 4b) is concentrated in the imaginary channel. At high frequencies (Figure 4c, inset), both Nyquist plots intercept the $Z_{Re}$ axis at ≈280 Ω, which is the series resistance of the PBF buffer solution. For the virus electrode, this 280 Ω solution resistance is in series with the 10 Ω resistance of the CVL. These data define the "baseline" impedance of the CVL against which changes associated with the binding of p-Ab (or n-Ab) will be measured.

**Optimizing the Detection of p-Ab.** How is the impedance of the virus electrode affected by exposure to a target molecule that it is capable of binding? The target molecule selected for this study, p-Ab, was an antibody to the P8 majority coat protein with a molecular weight of 148.5 kDa. p-Ab binds to free M13 in solution with an equilibrium constant, $K_D = k_d/k_a \approx 0.20$ nM, as shown previously.[4] We have recently[4] reported an investigation of the binding of p-Ab to the CVL using quartz crystal microbalance (QCM) gravimetry, and this study confirms that the CVL binds p-Ab with an apparent $K_D < 1$ nM. As a control, we employed a second antibody, "n-Ab", that shows no measurable affinity either for free M13 or for the CVL.

An initial look at the effect of these two molecules, p-Ab and n-Ab (both 67 nM), suggests that the effect of exposure to either is very slight for frequencies below 50 Hz (Figure 5a). In fact, this conclusion is incorrect: Since the total impedance at these frequencies is very high, even the small impedance shifts seen in Figure 5b correspond to hundreds of kilohms. At high frequencies, above 4 kHz (Figure 5c), n-Ab has little effect on the baseline impedance of the PBF buffer solution but p-Ab causes a small, ≈10 Ω increase in the resistance of the electrode while causing

(24) Marvin, D. *Curr. Opin. Struct. Biol.* **1998**, *8*, 150–158.
(25) Marvin, D.; Hale, R.; Nave, C.; Citterich, M. *J. Mol. Biol.* **1994**, *235*, 260–286.

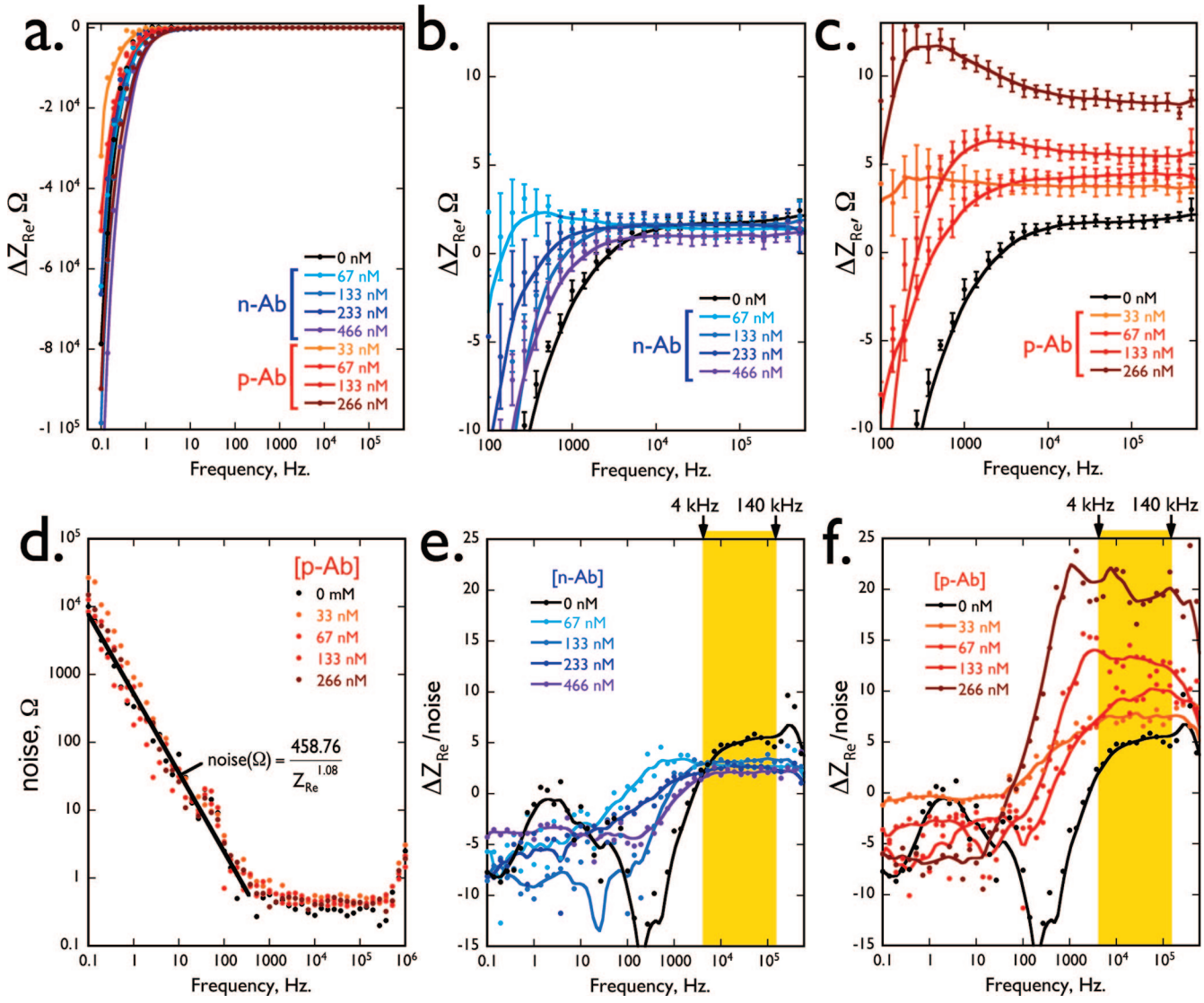


**Figure 6.** (a−c) $\Delta Z_{Re}$ versus frequency for the virus electrode in solutions of varying concentrations of p-Ab (red and orange) and n-Ab (blue and purple). In parts b and c, the $\Delta Z_{Re}$ data for frequencies above 100 Hz are shown. (d) Plot of noise versus frequency, where noise is defined as the standard deviation of $\Delta Z_{Re}$ for three consecutive measurements of the impedance spectrum using the same virus electrode. As is apparent here, these data are independent of the p-Ab concentration. Noise data for n-Ab fall on top of the p-Ab data shown here. (e,f) The $\Delta Z_{Re}$-to-noise (S/N) ratio, as defined in the text, as a function of frequency for solutions of (e) n-Ab and (f) p-Ab.

almost no change in its capacitance. Is this increase in $Z_{Re}$ correlated with the p-Ab concentration? To answer these questions, we take a closer look at the shifts in impedance, $\Delta Z_{Im}$ and $\Delta Z_{Re}$, caused by exposure to p-Ab and n-Ab across a range of concentrations.

The effect of n-Ab and p-Ab on $Z_{Re}$ is seen in Figure 6. The shifts in $Z_{Re}$ seen at low frequency in Figure 4b translate into large $\Delta Z_{Re}$ for both p-Ab and n-Ab, approaching 100 kΩ at 0.1 Hz. For both p-Ab and n-Ab, the resistance of the virus electrode is reduced upon exposure to the molecule (Figure 6a). Although it can not be discerned in Figure 6a, the increases in $\Delta Z_{Re}$ are well correlated with concentration for p-Ab but much more weakly correlated for n-Ab. At frequencies above 1 kHz (Figure 6b,c), $\Delta Z_{Re}$ is less than 20 Ω and in this frequency regime, clear differences between p-Ab and n-Ab are apparent. Measured $\Delta Z_{Re}$ values are virtually zero for n-Ab at all concentrations, but p-Ab shows a $\Delta Z_{Re}$ that varies from 2 to 10 Ω according to the p-Ab concentration. The reproducibility of the measured impedance was assessed by performing each impedance scan three times in succession and calculating a standard deviation for $\Delta Z_{Re} - \sigma_{\Delta Z_{Re}}$. A plot of $\sigma_{\Delta Z_{Re}}$ versus frequency for p-Ab (Figure 6d) shows that the precision of the $\Delta Z_{Re}$ measurement increases dramatically with increasing frequency, from $\sigma_{\Delta Z_{Re}} = 10$ kΩ at 0.1 Hz to $\sigma_{\Delta Z_{Re}} \approx 0.8$ Ω at 1 kHz, in direct proportion to $1/f$. At higher frequencies up to 200 kHz, this noise floor of 0.8 Ω is constant. The measurement "noise" revealed by replicate measurements shows no dependence on the p-Ab concentration or, indeed, on the concentration of n-Ab (data not shown). Systematic variations in the impedance measurement precision with frequency of the type seen here have not been reported previously, to our knowledge, but $1/f$ noise is a ubiquitous feature of electronic circuits, many types of frequency domain measurements, and some natural phenomena such as radioactive decay.

Which frequency is the most useful for determining the p-Ab concentration using $\Delta Z_{Re}$? $\Delta Z_{Re}$ is largest for frequencies below 1 Hz, but the noise present in the measurement is also a

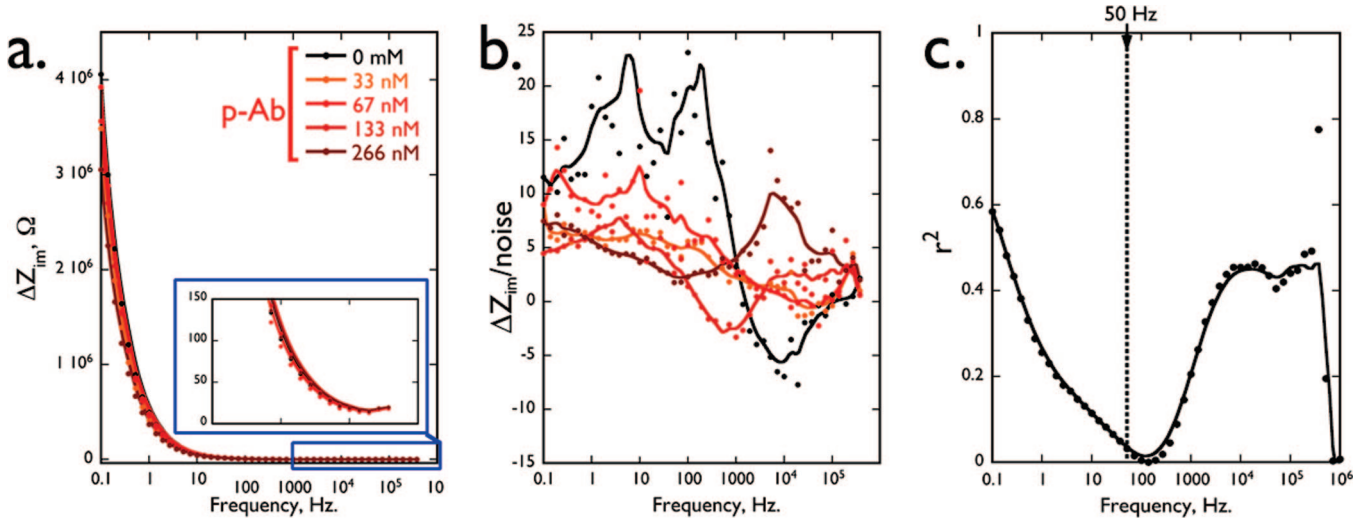


**Figure 7.** (a) $\Delta Z_{Im}$ versus frequency for the virus electrode in solutions of varying p-Ab concentration from 0 (PBF buffer) to 266 nM. (b) The $\Delta Z_{Im}$-to-noise (S/N) ratio, as defined in the text, as a function of frequency. S/N is uncorrelated with p-Ab concentration. (c) Plot of $r^2$, characterizing the correlation between p-Ab concentration and $Z_{Im}$, versus frequency.

maximum here. It is therefore reasonable to define a "signal-to-noise ratio" (S/N) as follows: $S/N = \Delta Z_{Re}/\sigma_{\Delta Z_{Re}}$. S/N defined in this way is plotted for n-Ab and p-Ab in Figure 6e,f, respectively. In these two plots, we highlight the frequency range from 4 to 140 kHz. Within this band, we measure S/N for n-Ab of <1, independent of the concentration, and a S/N for p-Ab that is proportional to its concentration, up to values of 20 at [p-Ab] = 266 nM. Outside of this frequency range, the S/N for pAb is smaller, more weakly correlated with concentration, and fluctuating widely with frequency.

In comparison to $Z_{Re}$, $Z_{Im}$ is useless for detecting p-Ab. A value for the S/N can nevertheless be calculated (Figure 7b), but it is very weakly correlated with p-Ab concentration. This can be seen most directly by calculating the correlation coefficient, $r$, for the dependence of $Z_{Im}$ on the p-Ab concentration at every frequency point. In Figure 7c, we plot $r^2$ versus frequency. The highest values of just $r^2 = 0.6$ are obtained near 0.1 Hz. Clearly, the capacitance of the electrode is little changed by the insertion of p-Ab into the CVL leading to the conclusion that the overall dielectric constant of the CVL is weakly affected by the incorporation of p-Ab. An equivalent circuit for the CVL quantitatively accounting for these observations is presented in the Supporting Information.

The correlation between $\Delta Z_{Re}$ and the p-Ab concentration exhibits greatest linearity at high and low frequencies. Setting aside the noise issue identified above, the sensitivity of this measurement is highest at low frequency (Figure 8a) where the CVL becomes less resistive with p-Ab loading. It equals 220 Ω $nM^{-1}$ at 0.1 Ω. At 50 Hz, the sensitivity for p-Ab detection is essentially zero, and at higher frequency, the CVL become more resistive with p-Ab loading (Figure 8b). The small $\Delta Z_{Re}$ seen at 1 kHz and above translates into low sensitivities of just 0.3 Ω $nM^{-1}$, almost 2 orders of magnitude lower than seen at the lowest frequencies. A plot of $r^2$ characterizing the correlation of $\Delta Z_{Re}$ and [p-Ab] is ≈0.9 below 10 Hz, and >0.95 above 4 kHz (Figure 8c). On the basis of the analysis presented in Figure 8a–c, one concludes that low frequencies are superior to high frequencies for the determination of p-Ab based on the greater sensitivity available, but this conclusion is incorrect because it leaves out the importance of selectivity. In Figure 8d, the virus electrode is incapable of distinguishing p-Ab from n-Ab at a frequency, 2 Hz, that is close to optimal in terms of sensitivity. As shown in Figure 8d, the virus electrode produces a highly linear calibration curve for p-Ab, but $\Delta Z_{Re}$ values at these frequencies are highly variable for both p-Ab and n-Ab leading to an apparent absence of selectivity and large error bars. The situation at 2 Hz is, in fact, no better than at 50 Hz where the sensitivity is close to zero (Figure 8e). The virus electrode is unable to distinguish between p-Ab and n-Ab at either frequency. Within the range from 4 to 140 kHz, however, much lower noise levels and higher S/N translate into an ability to distinguish between p-Ab and n-Ab, albeit with relatively low sensitivities for p-Ab (Figure 8f). We estimate a limit-of-detection for this measurement of 20 nM. This value is noise-limited and not dictated by $K_D$.

It should be emphasized here that the calibration plots of Figure 8d–f were obtained using 10 different virus electrodes, one for each value of p-Ab or n-Ab measured. This is because it was impossible to reuse an electrode for more than one concentration since the bound antibody could not be removed from the CVL. The data of Figure 8f is impressive when seen in this light since it suggests that the reproducibility of the CVL from electrode to electrode is very good. The direct implication is that a biosensor based on this surface chemistry and transduction scheme might require no calibration.

**On the Effect of HCl on the CVL.** We were surprised to discover that washing a virus electrode with 0.05 M HCl did not release the bound p-Ab and regenerate a "clean" virus electrode surface. In our prior work with CVLs,[4] we were able to release bound p-Ab from a CVL-modified gold quartz crystal microbalance (QCM) crystal in a flow cell and recover mass values that closely approximated the mass measured before p-Ab exposure. This p-Ab exposure and HCl wash sequence could be repeated up to 10 times to generate an entire calibration curve using a single CVL. As already indicated, this does not work with the virus electrode: Instead, exposure to 0.05 M HCl causes a immediate loss of sensitivity to p-Ab. Why are our observations regarding the effects of HCl so different in the context of QCM and electrochemical impedance when the phage attachment and recognition chemistry

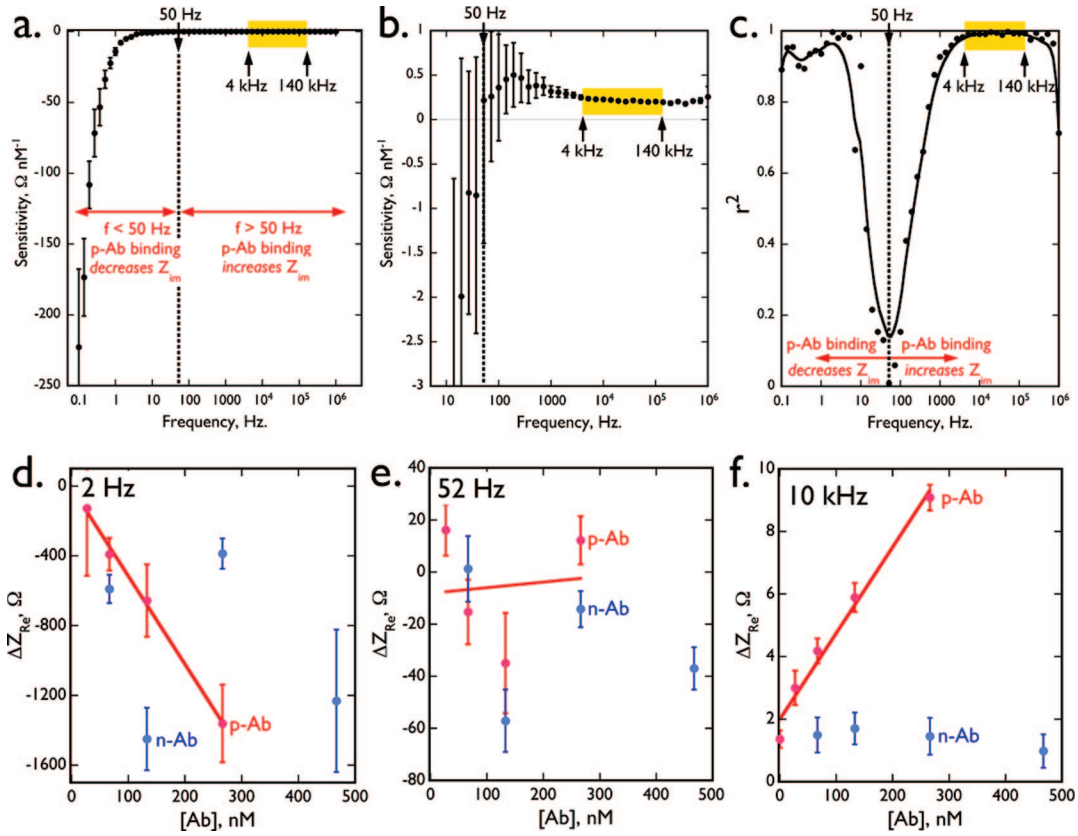


**Figure 8.** (a,b) Plots of the sensitivity to p-Ab, defined as $\Delta Z_{Re}$/concentration, versus frequency for the virus electrode. The sign of the sensitivity changes at 50 Hz because exposure to p-Ab causes a decrease in $Z_{Re}$ for lower frequencies and an increase in $Z_{Re}$ for higher frequencies. (c) Plot of $r^2$ characterizing the correlation between p-Ab concentration and $Z_{Re}$ versus frequency. In spite of the inversion in the sign of the sensitivity, the resistance is highly correlated with [p-Ab] at both low and high frequencies. (d−f) $\Delta Z_{Re}$ versus the concentrations of p-Ab and n-Ab plots for three frequencies, (d) 2 Hz, (e) 52 Hz, and (f) 10 kHz.

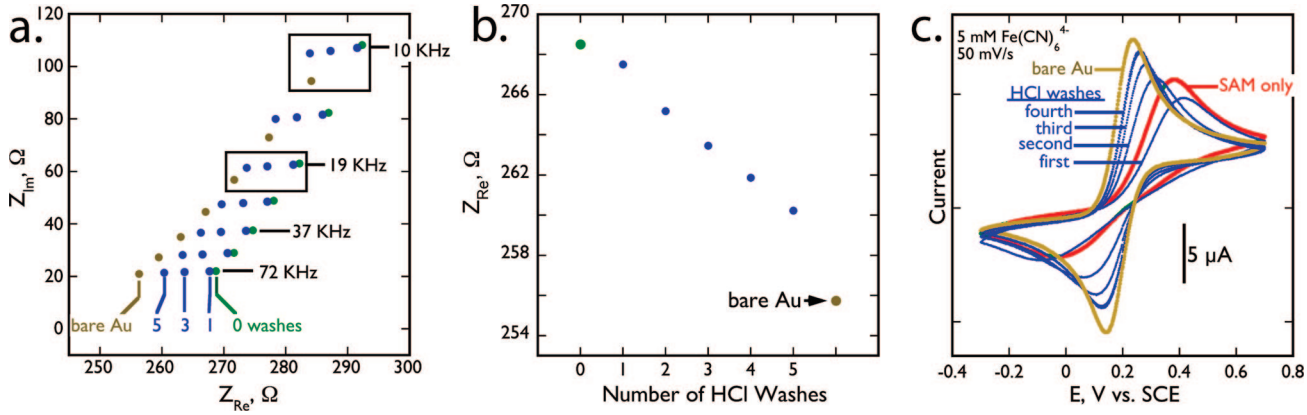


**Figure 9.** (a) The high-frequency impedance response of a freshly prepared virus electrode (green) and the responses measured after washing with 0.05 N HCl and 0.1% Tween 20 for multiple times as indicated. Also shown is the response of a bare gold electrode (yellow). (b) Plot of $Z_{Re}$ measured at 100 kHz for the experiments shown in part a. (c) Cyclic voltammograms (50 mV/s) for a freshly prepared SAM-modified gold electrode in a solution containing 5 mM $Fe(CN)_6^{4-}$ in PBF buffer (red) and the same electrode after washing with 0.05 M HCl up to four times (blue). Also shown is the voltammetry of a bare gold electrode in the same solution (gold).

are the same? We examined this issue in some detail, and a hypothesis emerges based upon the data presented next.

The loss of sensitivity caused by washing with 0.05 M HCl leads immediately to an erosion in the electrical resistance of the CVL. With successive washes, a progressive shift in $Z_{Re}$ to lower values is seen in the Nyquist plot at high frequency (Figure 9a), converging on the resistance of a bare gold electrode. After five washes, 60% of the initial resistance of the CVL has been lost (Figure 9b). Interestingly, repeated exposure of the CVL to 0.05 M HCl has little effect on the cyclic voltammetry of either $Ru(NH)_6^{3+}$ or $Fe(CN)_6^{4-}$ (Figure S2). In view of the data already presented in Figure 4, this is not a surprising result: In the case of $Ru(NH)_6^{3+}$, the voltammetry at a pristine CVL is already virtually identical to bare gold. In the case of $Fe(CN)_6^{4-}$, the voltammetry is unaffected because very little of this negatively charged complex is present within the negatively charged SAM

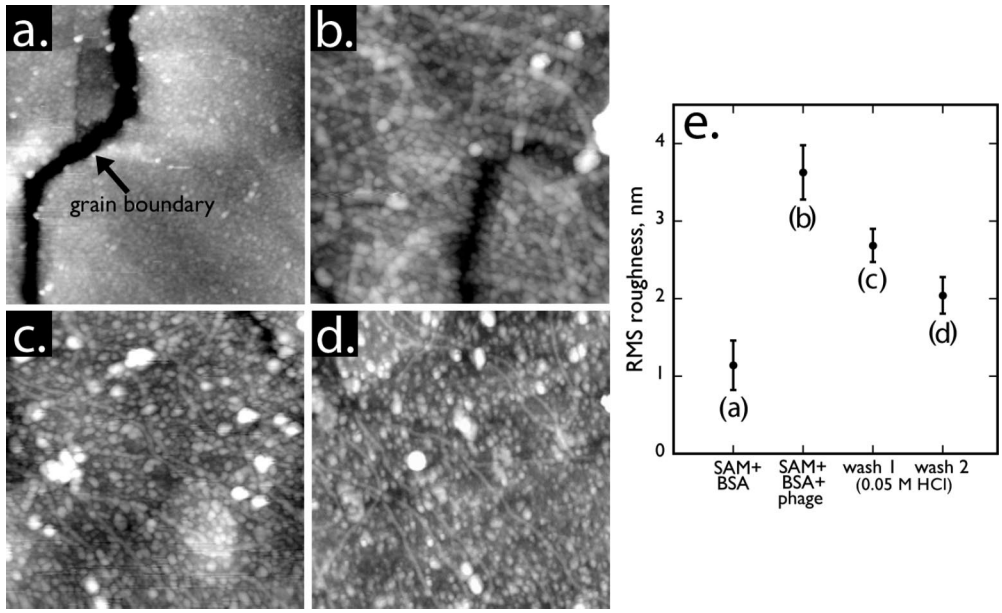


**Figure 10.** Ex-situ AFM images (a–d, 1 × 1 $\mu m^2$) acquired in air: (a) annealed gold electrode after assembly of the SAM and exposure to BSA. The fissure bisecting this image is a gold grain boundary. (b) Freshly prepared CVL, (c) CVL after one rinse in 0.05 M HCl, (d) CVL after two HCl rinses. (e) Plot of mean rms roughness for four different electrode surfaces as indicated. These data represent averages of four images acquired from different areas of the electrode selected at random, but areas with gross topographical defects such as grain boundaries were excluded from the analysis.

layer. Neither of these redox probes are sensitive indicators of the structural integrity of the CVL. However, the integrity of the SAM layer in the absence of attached phage can be probed by using $Fe(CN)_6^{4-}$ (Figure 9c). Peak currents are increased, and reversibility of the voltammetry is improved with successive washes of the SAM layer with 0.05 M HCl, providing clear evidence for the removal of the SAM layer.

The erosion in the electrical resistance of the CVL suggests that it is removed by the 0.05 M HCl, but the defects produced by this process are not readily visible in AFM images of the virus electrode surface (Figure 10). An AFM image of a freshly prepared virus electrode surface (Figure 10a) shows linear features assigned to phage particles or bundles of phage particles. In addition, spheroid particles are also seen on these surfaces. After washing once (c) and twice (d) with 0.05 M HCl, AFM images show a larger number of spheroid particles and fewer linear strands. In spite of the emergence of these spheroid particles, the overall rms surface roughness is decreased after each washing (Figure 10e). Elimination of BSA from the prep did not alter the number of particles observed after HCl washing of these surfaces. On the basis of this analysis, both the spheroid particles and the linear strands are derived from the filamentous M13 phage particles.

What mechanism can account for the apparent loss of extended phage particles and the formation of these spheroid particles? We explored the possibility that exposure to acid could cause this transformation by inducing phage particles to transition from an extended to coiled conformation. Dynamic light scattering (DLS) was used to probe the hydrodynamic diameter of phage particles in buffered solutions as a function of pH (Figure 11). At pH = 7.2, two populations of phage particles are observed with hydrodynamic diameters of ≈100 nm and ≈1 $\mu$m. The latter mode corresponds to the expected length of M13 phage particles and therefore represents an extended conformation for these particles. As the pH is reduced to 4.5, a pronounced broadening is observed

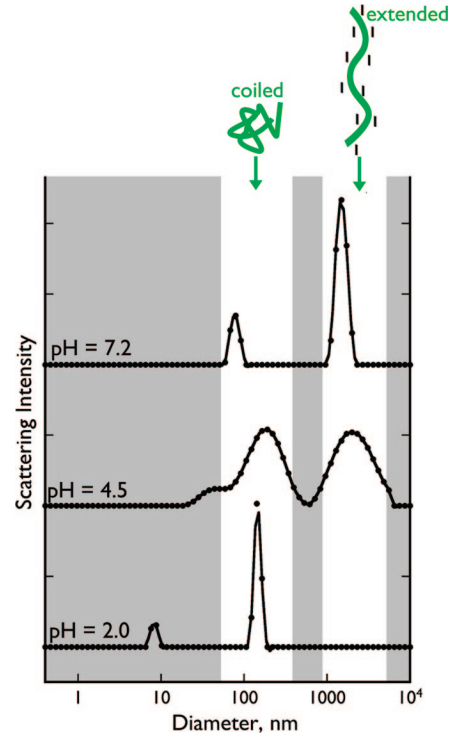


**Figure 11.** Dynamic light scattering intensity versus hydrodynamic diameter for solutions of M13 (50 nM) in 1 mL of PBS-Tween solution at pH 2.0, 4.5, and 7.2, as indicated.

in both of these modes, and with a further reduction in pH to 2.0, the 1 $\mu$m disappears completely and an increased intensity is observed for the ≈100 nm mode, which also becomes narrower. As shown schematically in Figure 11, the preferred state for M13 at pH = 7.2 is an extended rod as a consequence of the large negative charge density on the surface of the M13. As the pH is reduced to the PI of the virus, this negative charge density is

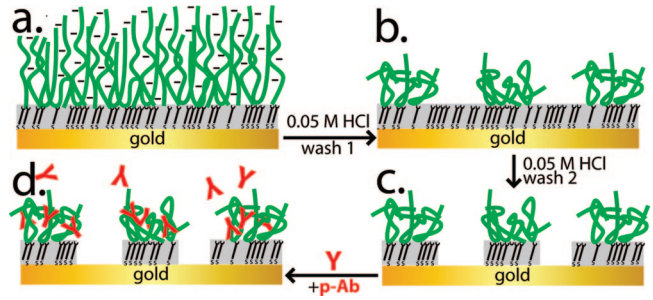


**Figure 12.** Proposed evolution of CVL structure caused by exposure to 0.05 M HCl and resulting in a loss of sensitivity for EIS detection of p-Ab.

reduced or eliminated, removing a barrier to the folding of the M13 into a coiled state.

The data of Figure 11 suggests that this extended to coiled transformation happens to M13 in solution. On the basis of this observation, a mechanism for the loss of sensitivity caused by HCl exposure of the CVL is the following (Figure 12): (a) At physiological pH, the negative change of M13 phage particles favor an extended rod conformation within the CVL. (b) After the first exposure of the CVL to 0.05 M HCl, negative charge on these phage particles is reduced or eliminated inducing a rod-to-coiled transition of the M13. The mechanical stresses imparted by the phage particles to their SAM attachment points causes detachment of some M13 from the monolayer, as seen in the AFM images of Figure 10. (c) Additional exposures to 0.05 M HCl cause the formation of pinholes at exposed regions of the SAM layer. These pinholes "short" the CVL reducing its apparent impedance, just as seen in Figure 9. The resulting surface (d) continues to show mass sensitivity to p-Ab binding, as previously reported.[4]

## SUMMARY

The main conclusions of this study are the following: (1) The CVL adds a frequency-dependent impedance, $Z_{total}$, to the impedance of a bare gold electrode. $Z_{total}$ is just 10 Ω from 4 kHz to 1 MHz but more than 1 MΩ at 0.1 Hz. Electrochemical processes characteristic of a bare gold electrode, including hydrogen evolution and oxide formation, are absent in the cyclic voltammetry of the virus electrode. The CVL, which is negatively charged, suppresses the electrochemistry of $Fe(CN)_6^{3-/4-}$ present in the buffer phase but the electrochemistry of $Ru(NH)_6^{2+/3+}$ is hardly affected. Collectively, these data suggest that M13 phage particles are tethered to a highly defective SAM layer. This assembly imposes little electrical resistance at high frequency, but the negatively charged phage layer is sufficiently dense to exclude $Fe(CN)_6^{4-}$ by Donnan exclusion. (2) Within a frequency band from 4 to 140 kHz, the small resistance imposed by the CVL increased significantly relative to the 10 Ω baseline upon exposure to p-Ab at concentrations above 20 nM. This resistance change of up to 10 Ω was directly proportion to the concentration of p-Ab. The mechanism for this resistance increase is likely the removal of free volume within the CVL layer by bound p-Ab and the concomitant elimination and/or constriction of the pathways available for ionic conduction. The resistance of the CVL is not affected at all by exposure to the nonbinding antibody n-Ab in this frequency range. (3) Exposure to p-Ab also caused changes in the low frequency impedance (<1 Hz) where it induced a decrease in resistance by up to 100 kΩ again in direct proportion to the p-Ab concentration. The amplitude of this resistance change was large but highly variable from measurement-to-measurement even with the same electrode in the same solution of p-Ab. The CVL could not reliably distinguish between p-Ab and n-Ab in this frequency range, also as a consequence of the trial-to-trial "noise" implicit in the measurement. The mechanism for this resistance decrease must be associated with a reduction in the charge transfer resistance imposed by the CVL, perhaps caused by mechanical strain on the CVL imposed by the incorporation of p-Ab into the CVL, but we have no independent confirmation for this. (4) The capacitance of the virus electrode was weakly correlated, or uncorrelated, with p-Ab binding at all frequencies in the range from 0.1 Hz to 1 MHz. The implication is that the dielectric constant of the protein-based CVL is insensitive to the incorporation of the protein p-Ab. (5) The measurement-to-measurement reproducibility of the frequency shift caused by p-Ab binding is strongly frequency dependent. The standard deviation for replicate impedance measurements, $\sigma_{\Delta Z}$, increases in proportion to $1/f$ from $\approx 10^5$ Ω to <1 Ω as the frequency is decreased from 2 kHz to 0.1 Hz. To first order, this "noise" was independent of phase and independent of the presence or absence of p-Ab or n-Ab. The preferred frequency range, 4 −140 kHz, corresponded to a frequency-independent noise "floor" of less than 1 Ω. (6) HCl (and other acids) cannot be employed to effect the release of bound p-Ab from the CVL as in our previous QCM study.[4] Exposure to 0.05 M HCl irreversibly damages the CVL for the detection by EIS of p-Ab. Our data suggests, but does not prove, that this damage may result from the mechanical stresses imparted to the CVL resulting from a conformational transition of the M13 virus from an extended rod conformation at pH = 7.2 to a coiled state at low pH.

On the basis of the results presented here, the virus electrode shows significant potential as a new platform for immunosensing. However, three problems must be solved in order to advance the concept of electrochemical detection using bioaffinity layers based upon whole viruses: First, the sensitivity of the EIS transduction must be improved. Much larger resistance changes will be needed to achieve $K_D$-limited concentration measurements. Second, the impedance contribution of the electrolyte must be eliminated in the EIS measurement of the phage layer. In this study, we carefully controlled the resistance of the electrolyte in order to observe the signals associated with p-Ab binding. The utility of the virus electrode concept will be limited if this continues to be a constraint of its use. Finally, to access the concentration range below $K_D$, a strategy for amplifying the effect of binding on the EIS signal must be developed.

## ACKNOWLEDGMENT

R.M.P. acknowledges funding support from the National Science Foundation (Grant CHE-0641169) and the Petroleum Research Fund of the American Chemical Society (Grant 46815-AC 10). G.A.W. acknowledges funding support from the NSF (Grant EF-0404057).

## SUPPORTING INFORMATION AVAILABLE

Additional information as noted in text. This material is available free of charge via the Internet at http://pubs.acs.org.

Received for review April 22, 2008. Accepted June 15, 2008.

AC8008109